

APPLIED SCIENCES AND ENGINEERING

High-voltage water-scarce hydrogel electrolytes enable mechanically safe stretchable Li-ion batteries

Peisheng He¹, Jong Ha Park¹, Yingkai Jiao¹, Rushil Ganguli¹, Yigen Huang¹, Ashley Lee¹, Christine Heera Ahn¹, Monong Wang², Yande Peng¹, Yu Long¹, Chun-Ming Chen¹, Zihan Wang¹, Ziting Tian³, Baoxia Mi², Ana Claudia Arias⁴, Chao Fang^{5*}, Anju Toor^{3*}, Liwei Lin^{1*}

Soft Li-ion batteries, based on conventional organic electrolytes, face performance degradation challenges due to moisture penetration and safety concerns due to possible leakage of toxic fluorine compounds and flammable solvents under mechanical damage. We design a water-scarce hydrogel electrolyte with fluorine-free lithium salt to achieve wide electrochemical stability window (up to 3.11 volts) in ambient air without hermetic packaging while balancing high stretchability (1348%), ion conductivity (41 millisiemens per centimeter), and self-healing capabilities for mechanically and chemically safe stretchable Li-ion batteries. Molecular synergy between hydrophilicity and lithiophilicity of zwitterionic polymer backbone is revealed by molecular dynamics simulations. The battery exhibits capacity retention under harsh mechanical stresses—enduring stretching, twisting, folding, and multiple through-punctures by a needle—while self-healing from repeated through cuts by a razor blade. Stable ambient operation for 1 month over 500 charge-discharge cycles (average coulomb efficiency, 95%) is achieved. A prototype self-healing electronic system with embedded soft batteries demonstrates practical application as a durable embodied energy source.

INTRODUCTION

Safe and stretchable soft batteries are desirable for applications in wearable electronics, soft robots, and the Internet of Things (1–4). However, most commercial Li-ion batteries are hermetically sealed with non-stretchable packages to prevent (i) the penetration of moisture that degrades performances (5) and (ii) the leakage of toxic and flammable electrolytes. Recently, deformable/stretchable batteries using conventional organic electrolytes without rigid packages have been reported (6–8) with good stretchability, but they often suffer from performance degradations in the ambient environment due to moisture penetration issues (6, 7, 9), resulting in short operational lifetime. Because the elasticity modulus and moisture permeability of the packaging material are two coupled and opposite factors (Fig. 1A) (10, 11), there is no good solutions for packaging these batteries.

Hydrogels exhibit attractive properties as a quasi-solid-state electrolyte. Water being the solvent, it is inherently less sensitive to moisture and nonflammable while exhibiting good stretchability and ion conductivity. However, although stretchable aqueous batteries with hydrogel electrolyte have been reported with good stretchability and cycle stability in the ambient (12–16), one key drawback is the narrow electrochemical stability window (ESW) of 1.23 V due to the water electrolysis process. As such, the selection of cathode and anode pairs are limited, and most reported stretchable aqueous batteries are predominantly based on zinc-ion chemistry and show relatively low

operation voltage compared to commercial Li-ion batteries (1, 16–21). The “water-in-salt” (WiS) electrolyte reported in 2015 opens up investigations into highly concentrated aqueous electrolytes containing almost no “free” water molecules (22–26) and gels with incorporated WiS electrolytes (27–29). A key limitation is that highly fluorinated lithium salts such as lithium bis(tri-fluoromethanesulfonyl)imide are heavily loaded in those electrolyte, which is highly toxic to human, expensive, and environmentally persistent (30).

Herein, a water-scarce hydrogel electrolyte with a wide voltage stability window is developed consisting of zwitterionic polymer backbone controllably loaded with fluorine-free lithium salt. A low content of water bound to the hydrogel is maintained via equilibrium with ambient moisture such that the electrolyte can function with a wide ESW without a hermetic rigid package (Fig. 1B). For example, experimental results show ~19 wt % water content can be maintained in the hydrogel under an ambient relative humidity (RH) of 50% to enable a high ESW of ~2.97 V, which matches that of those WiS electrolytes. The water-scarce zwitterionic hydrogel (WZH) retains key mechanical properties of conventional hydrogels such as high stretchability (1348% fracture strain) and self-healing capability against mechanical damages. A full Li-ion cell composed of rigid packaging and WZH electrolyte pre-equilibrated in the ambient with a RH of 50% can operate continuously over 2 months for 200 charge-discharge cycles at a charge/discharge rate of 0.2 C to achieve an average coulombic efficiency (CE) of 97%. As a proof of concept, a stretchable Li-ion battery prototype with a non-hermetic elastomer package shows good capacity retentions under harsh mechanical stresses, including folding, twisting, 50% stretching strain, and penetrations by a needle five times at different locations. By using a self-healable elastomer package, the deformable battery can self-heal itself from repeated through cuts by a razor blade and retain 90% of the original capacity. Meanwhile, the stretchable battery without hermetic packaging operates stably for 1 month in the ambient for 500 charge-discharge cycles with an average coulomb efficiency of 95%. To demonstrate its potential applications, a self-healable electronic system is constructed

¹Department of Mechanical Engineering and Berkeley Sensor & Actuator Center, University of California, Berkeley, Berkeley, CA 94720, USA. ²Department of Civil and Environmental Engineering, University of California, Berkeley, Berkeley, CA 94720, USA. ³School of Materials Science and Engineering, Georgia Institute of Technology, Atlanta, GA 30332, USA. ⁴Department of Electrical Engineering and Computer Sciences, University of California, Berkeley, Berkeley, CA 94720, USA. ⁵Sustainable Energy and Environment Thrust and Guangzhou Municipal Key Laboratory of Materials Informatics, The Hong Kong University of Science and Technology (Guangzhou), Guangzhou 511400, Guangdong, China.

*Corresponding author. Email: chaofang@hkust-gz.edu.cn (C.F.); anju@gatech.edu (A.T.); lwlin@berkeley.edu (L.L.)

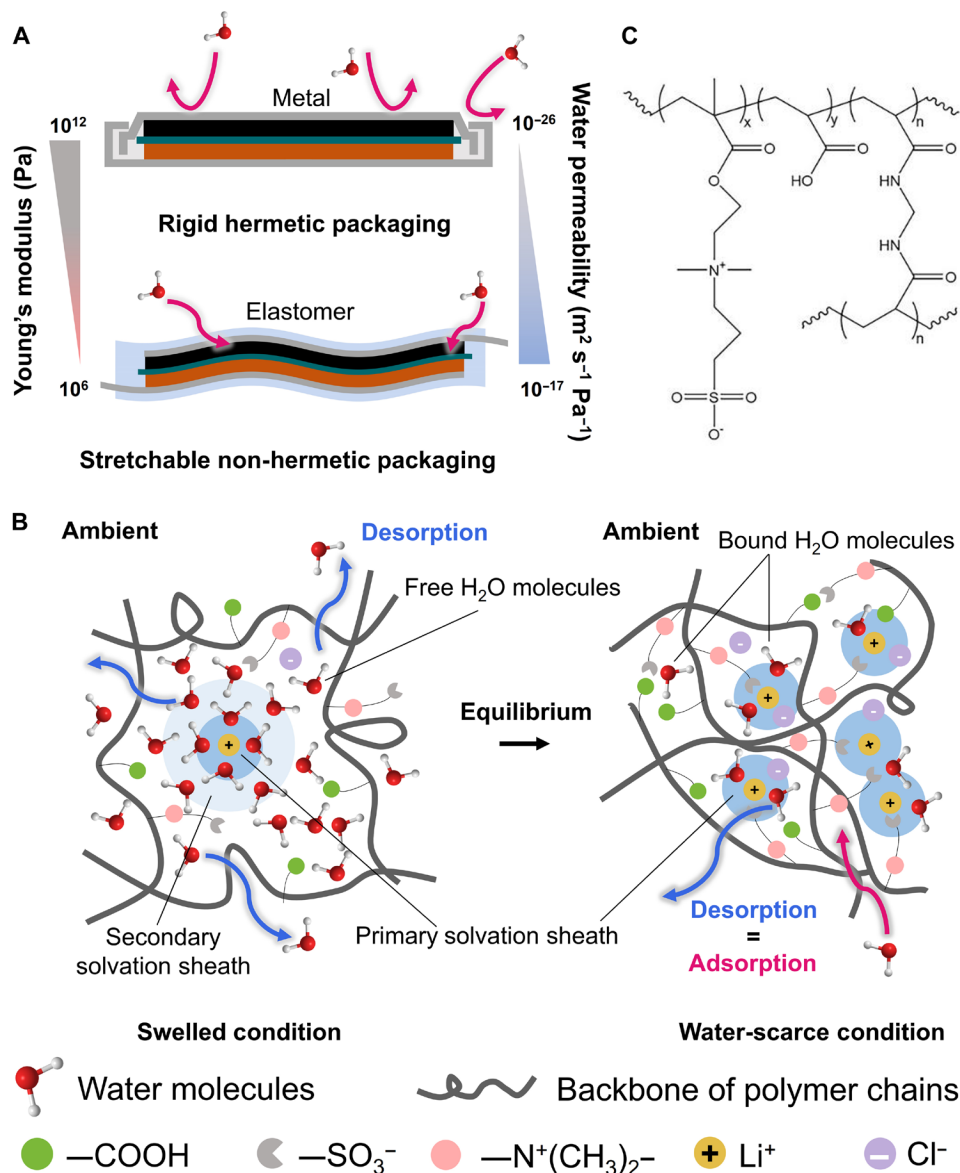


Fig. 1. Mechanically safe and stretchable Li-ion battery with WZH electrolyte. (A) Schematic comparison of a typical coin-cell Li-ion battery with the hermetic metal package and a stretchable battery with the non-hermetic elastomer package. Rigid metal has high Young's modulus with low water permeability, while elastomer has low Young's modulus and high water permeability, which can degrade the battery performance. (B) Illustration of the lithium solvation shell in the zwitterionic hydrogel under swelled condition and water-scarce condition. The water-scarce condition is realized in the hydrogel by controllably loading the fluorine-free lithium salt LiCl to zwitterionic polymer backbone such that a low content of water is adsorbed in equilibrium with the ambient moisture. This allows for the hydrogel electrolyte to stably maintain a wide stability window in the ambient and be functional as a water-scarce electrolyte in a battery without the hermetic rigid package. (C) Chemical structure of the water-scarce zwitterionic hydrogel (WZH) polymer backbone synthesized in this work.

consisting of the soft battery and an electronic circuit that can recover from a through-cut damage and remain operational highlighting the high mechanical safety under extreme mechanical damages.

RESULTS

WZH electrolyte

The proposed WZH electrolyte (Fig. 1C) is synthesized by a one-pot free-radical copolymerization process in a LiCl solution. In the process, the [2-(methacryloyloxy)ethyl] dimethyl-(3-sulfopropyl)

ammonium hydroxide (MEDSAH) is used as the zwitterionic monomer and acrylic acid (AA) as the hydrogen-bond donor, with *N,N'*-methylenebisacrylamide (MBAA) serving as the covalent cross-linker (fig. S1). After the synthesis process, the hydrogel is equilibrated in a chamber with a fixed humidity level.

Conventional hydrogel electrolytes operate under high water contents to ensure good ion conductivity but suffer from limited ESW as the solvation shell of lithium ion is dominated by the hydration water and free water molecules are prevalent as illustrated in the swelled condition in Fig. 1B. On the other hand, if hydrogels are

completely dehydrated, then ions and polymer chains are highly confined, resulting in low ion conductivity and high rigidity. The water-scarce hydrogel system developed in this work overcomes this limitation by operating with low moisture content in equilibrium with the ambient environment. Specifically, by controllably loading hygroscopic lithium salt, the amount of moisture adsorbed from air to the hydrogel can be modulated. On one hand, the adsorbed water molecules compete with functional groups on the polymer backbone for association with Li-ions, thereby releasing Li-ions from the polymer backbone for good ion mobility. On the other hand, the adsorbed moisture content is limited as such that adsorbed water molecules are mostly bound to ions or polymer backbones as such that the reactivity of water is largely suppressed to achieve wide ESW. Dynamic vapor sorption (DVS) tests show that WZH electrolyte uptakes much less water content compared to pure LiCl salt under different humidity levels (Fig. 2A) and typically contains only ~19 wt % of water under a RH of 50% (fig. S2), which is substantially lower than those in conventional hydrogel (water content typically >80 wt %) (31).

To ensure good hydrogel stability under water-scarce conditions, the polymer backbone is designed with a high affinity for both lithium salt and water. Here, the zwitterionic backbone consisting of quaternary ammonium cation and sulfonic anion group (fig. S1) is used for good hydrophilicity and the dissociation with salt due to the anti-polyelectrolyte effect (32). Previous studies (31, 33) have shown that the negatively charged sulfonic group exhibits high affinity to lithium ion, while the anion part of the lithium salt can be readily dissociated by the positively charged quaternary ammonium group. In addition to the zwitterionic monomer, carboxylic acid

groups are introduced to the polymer backbone by copolymerizing the AA as a hydrogen bond donor. The interaction between AA and zwitterionic group leads to the synergistical increase of the polymer backbone solubility in water due to strong hydrogen bonding (34, 35) similar to those reported in deep eutectic solvent systems. This helps the formation of a homogeneous system with a high salt concentration in favor of battery operations without the phase separation. In addition, the carboxylic acid group also helps to enhance the reversible bonding between polymer chains, thereby rendering WZH with good self-healing capability.

Horizontal attenuated total reflectance–Fourier transform infrared spectroscopy (HATR-FTIR) (Fig. 2B and fig. S3) and Raman spectroscopy (Fig. 2C and fig. S4) are used to investigate the molecular interactions between water, LiCl, and the polymer backbone in the as-synthesized hydrogels. For pure water, the O–H stretching of the water molecules is characterized by a broad band at a wave number around 3294 cm^{-1} , indicating the existence of multiple different hydrogen bonding environments within the water clusters (36, 37). For WZH electrolytes, the band narrows substantially, corresponding to an increase in polymer-bond and hydration water population at the expense of free water molecules. The peak in the FTIR spectra also blue shifts from 3294 cm^{-1} of pure water to 3359 cm^{-1} and further to 3385 cm^{-1} as water content decreases, which is indicative of strengthened covalent O–H bonds (38). These results suggest the disruption of the hydrogen bond network between water molecules due to enhanced interactions between water molecules and functional groups on zwitterionic backbones via hydration and hydrogen bonding. This could suppress the fast proton transport through the Grotthuss diffusion mechanism (39), thereby reducing the hydrogen evolution

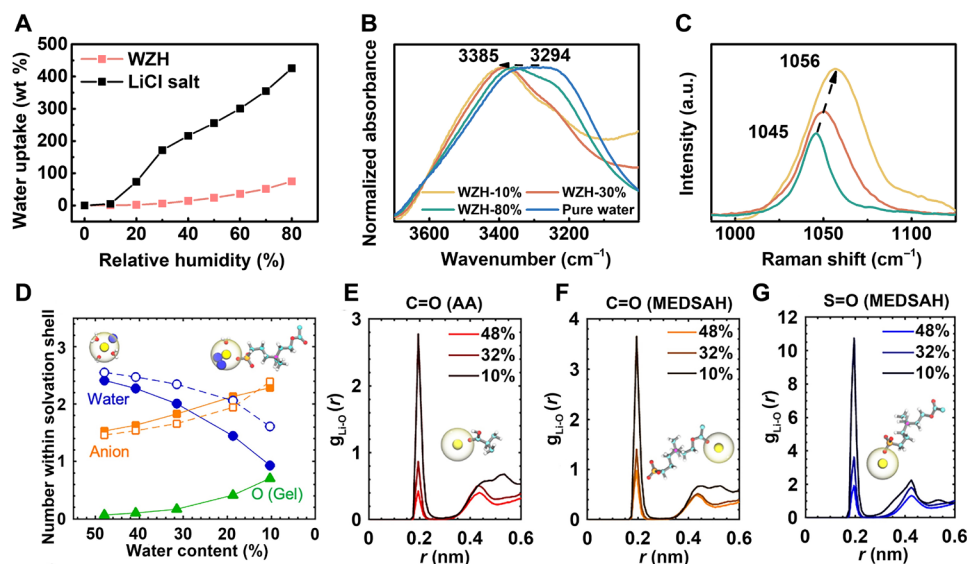


Fig. 2. Spectral characterization and solvation structure analysis of the hydrogel electrolyte. (A) Water uptake of WZH electrolyte and LiCl salt from RH of 0 to 80%. (B) The O–H stretching region of the FTIR spectra. (C) The S=O stretching region of the Raman spectra for the zwitterionic hydrogel with different water contents (10, 30, and 80 wt %). a.u., arbitrary units. (D) Evolution of the number of water molecules, anions, and oxygens from the gels within the first solvation shell of Li^+ as a function of water content. Data with solid symbols and lines represents the number of water molecules, anions, and oxygens in the case of WZH electrolyte, while open symbols and dashed lines represent pure LiCl/water system at the same mole of salt per kg water. The left and right inset snapshots, respectively, show typical snapshots of Li^+ (in yellow spheres) solvation shell at a water content of 50 and 10 wt %. The solvation shells are represented by large transparent spheres. Cl^- ions are represented in blue spheres. Water molecules and the zwitterionic sub-chain are shown in ball-and-stick model with bonds in white, carbon in cyan, nitrogen in purple, oxygen in red, and sulfur in orange. Pair correlation functions between Li^+ and double-bonded oxygen atoms [$g_{\text{Li-O}}(r)$] of (E) C=O from AA, (F) C=O from MEDSAH, and (G) S=O from MEDSAH at different water contents. The insets in (E) to (G) depict the solvation of Li^+ involving the three types of groups from gels.

reactions for an extended ESW. Meanwhile, as the hydrogel transition from the swelled state to water-scarce condition, S=O stretching vibration of the $-\text{SO}_3^-$ group in WZH electrolyte also shows a notable blueshift both in Raman (Fig. 2C; from 1045 to 1056 cm^{-1}) and FTIR (fig. S3B; from 1043 to 1047 cm^{-1}) spectra, implying the enhanced interaction between sulfonic group with cationic groups. The C=O stretching vibration band also shifts from 1721 cm^{-1} to a higher wave number of 1727 cm^{-1} in the Raman spectra as the water content reduces (fig. S4), which further confirms the enhanced hydrogen bonding interactions (40). The evolution of microscopic solvation structure of Li^+ in the WZH electrolyte with water content is further revealed via the molecular dynamics (MD) simulation of the hydrogel system (Materials and Methods and figs. S5 to S9). The model system consists of a three-dimensional (3D) gel network, water molecules, and LiCl salts, as shown in fig. S6. We examine the composition of the primary Li^+ solvation shell as a function of water content in Fig. 2D. For the hydrogel with water content of $\sim 50\text{ wt}\%$, the Li^+ solvation shell comprises 2.4 water molecules (the blue line with solid symbols) and 1.5 anions (the orange line with solid symbols), which approaches that of pure water/LiCl system (dashed lines with open symbols) under the same molality. The left and right snapshots, respectively, show typical snapshots of Li^+ solvation shell at a water content of 50 and 10 wt %. As the water content reduces, the system transitions from the swelled state to water-scarce state, and the Li^+ is solvated by more anions but fewer water molecules. The number of water molecules deviates more substantially from the pure water/LiCl system at low water content: Li^+ in WZH electrolyte is solvated by ~ 0.7 fewer water molecules than in the pure water/LiCl system at the lowest water content ($\sim 10\text{ wt}\%$). Such reduction in the number of Li^+ -coordinated water molecule is caused by the prevalence of polymer-water interaction at low water content (31), i.e., a relatively larger population of water molecules form bonds with gel backbone (see Supplementary Text and figs. S8 and S9). As a result, more anionic moieties of polymer backbone can enter the solvation shell of Li^+ in place of water, which is schematically revealed by the right inset in Fig. 2D. The reduction of the number of water molecules in Li^+ solvation shell could potentially contribute to a wider ESW (26, 30, 41, 42).

To further investigate the functional groups accounting for the interaction between lithium ion and the zwitterionic polymer backbone, pair correlation functions between lithium ions and double-bonded oxygens with respect to distance r , $g_{\text{Li}-\text{O}}(r)$, of C=O from AA, C=O from MEDSAH, and S=O from MEDSAH are shown in Fig. 2 (E to G), respectively. The intensification of the interaction between Li^+ and these groups, as water content decreases, is marked by the progressively increasing height of the first peaks of pair correlation functions, which agrees well with the blue shifts in S=O stretching and C=O stretching vibrations observed in FTIR and Raman spectra. Notably, S=O exhibits a much higher peak in $g_{\text{Li}-\text{O}}(r)$, indicating the stronger interaction between S=O and Li^+ (and water), which corresponds to a more pronounced blue shift in Raman spectrum of the S=O stretching band (Fig. 2C) as compared to that of the C=O stretching band (fig. S4B).

Electrochemical and mechanical properties of WZH electrolyte

The ESWs of WZH are evaluated by linear scanning voltammetry in a three-electrode setup. Screen-printed carbon electrodes (RRPE 1001C, Pine Research Instrumentation) are used as the working and counter electrodes and Ag/AgCl as the reference electrode. All hydrogel

samples are pre-equilibrated in a chamber with RH of $\sim 50\%$, under which the measured ESWs show good consistency across different samples (table S1). Figure 3A shows the increase of zwitterionic monomer MEDSAH content expanded the ESW from 2.73 V for WZH-1 (MEDSAH/AA monomer ratio of 1:2) further to $\sim 2.97\text{ V}$ for WZH-2 (MEDSAH/AA monomer ratio of 1:1). This is substantially higher than the $\sim 1.8\text{-V}$ window of a conventional polyacrylic acid electrolyte with LiCl addition (PAA-LiCl) and wider than that of a saturated LiCl solution due the strong Li^+ affinity from the zwitterionic moieties on the polymer backbone, agreeing with the spectral analysis and MD simulations results. The incorporation of these moieties into the solvation shell further reduces the water content in the Li^+ solvation structure and leads to expanded ESW. While some improvements in ESW are found by further increasing the MEDSAH/AA ratio to 2:1 (fig. S10), the hydrogel becomes rigid and the ionic conductivity drops considerably (fig. S11) due to the strong self-association between zwitterionic groups on the polymer backbone. Therefore, WZH electrolyte with MEDSAH/AA weight ratio of 1:1 is used for further investigation in the rest of this paper unless otherwise noted. The impact of humidity variations on ionic conductivity and ESW is also studied. When RH is reduced to RH of 30%, the hydrogel still maintains an ion conductivity of 0.6 mS cm^{-1} (Fig. 3B), while ESW is slightly extended from 2.97 V at RH of 50% to around 3.11 V (fig. S12). This is mainly due to the reduced equilibrium water content of WZH at decreased humidity. As previously shown in fig. S2, the water content of the hydrogel decreases from 19 wt % at RH of 50% to around 5.7 wt % at RH of 30%. As such, fewer water molecules can participate in the solvation of lithium ion. Conversely, an

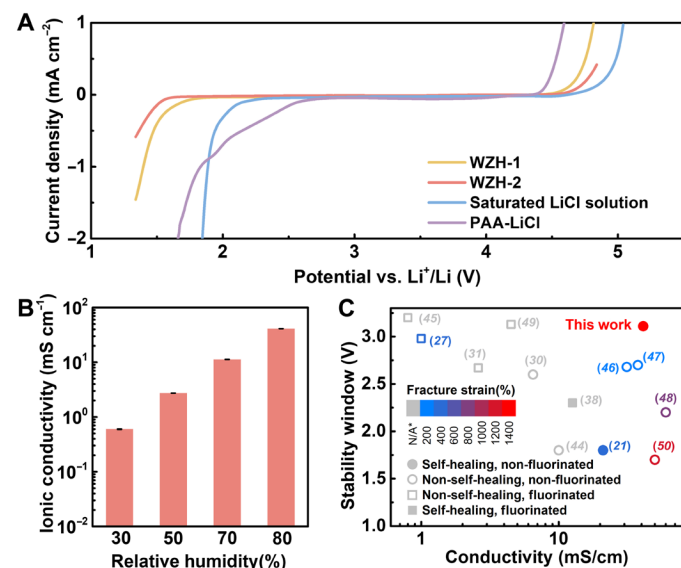


Fig. 3. Hydrogel electrolyte characterizations. (A) Comparison of ESWs of WZHs with different MEDSAH/AA monomer ratios (by weight, 1:2 for WZH-1 and 1:1 for WZH-2), saturated LiCl solution, and PAA with incorporated LiCl, measured by linear scanning voltammetry at 10 mV s^{-1} with printed carbon electrodes as working and counter electrodes and Ag/AgCl as the reference electrode. The potential values are converted to the Li/Li^+ reference for convenience. (B) Ionic conductivities of WZH-2 at different RH levels. (C) Comparison between this work and other reported aqueous hydrogel electrolytes (21, 27, 30, 31, 38, 44–50) in terms of room temperature ion conductivity, ESW, fracture strain, self-healability, and fluorine content. *N/A (not applicable): Fracture strain of electrolyte is not reported for these works (30, 31, 38, 45, 49).

elevation of humidity from RH of 50 to 70% leads to four times increase in conductivity and slight reduction of the ESW by 0.2 V due to an increase in water content (33.9 wt % at RH of 70%). Overall, because the water content of WZH electrolyte remains relatively low (<43 wt %) within the tested humidity range (RH of 0 to 80%), the solvation shell of lithium ion mostly consists of anions and zwitterionic groups under such water-scarce condition (Fig. 2D), which leads to a wide ESW over a wide range of humidity level. However, when the humidity level drops below RH of ~20%, the WZH becomes too rigid to establish good contacts with electrodes. This could be potentially addressed by inducing an additional hydrogen bond donor to the system to form deep eutectic solvent-based ionogel for better ionic conductivity at low humidity conditions due to their low vapor pressure (43). The typical stress-strain curve of the resulting WZH electrolyte is shown in fig. S13. The hydrogel exhibits a tensile strength of 407 ± 57 kPa and a low modulus of around 353 ± 73 kPa that matches human epidermis (140 to 600 kPa). Due to the presence of the multiple sets of physical cross-links such as ionic interactions and hydrogen bonding, the resulting WZH hydrogel shows high stretchability of 1348%. Cyclic tensile tests are performed to further characterize the mechanical properties of the hydrogel (fig. S14). Noticeable hysteresis is observed, and the dissipation ratio, defined as the dissipation energy loss (represented by the hysteresis area) over the total work of external forces, is calculated to be around 67%. This highlights the abundant physical cross-links in the WZH hydrogel network. During deformation, they rupture to help dissipating deformation energy, while the process is reversible with good cyclic stability over 10 cycles under a large strain of 200% in prototype tests. Figure 3C compares WZH and other aqueous hydrogel electrolytes in terms of mechanical and electrochemical properties, self-healing capability, and fluorine content. Notably, WZH exhibits the highest stretchability while maintaining a wide ESW (up to 3.11 V) and good ion conductivity (up to 41 mS cm^{-1}) in the ambient, surpassing most reported works (27, 30, 31, 38, 44–50). Moreover, the self-healing capability and non-fluorinated composition enhance both mechanical and chemical safety against potential damages. These attributes make the hydrogel a promising candidate as electrolyte for deformable batteries that can seamlessly and safely interface with human skin.

Cyclic voltammetry (CV) is used to investigate the expanded ESW of the WZH electrolyte with LiMn_2O_4 (LMO) as the cathode and V_2O_5 as the anode, respectively, in a three-electrode setup. LMO is selected because of its relatively high lithiation/de-lithiation potential that can maximize the stability window of WZH electrolyte (up to ~4.6 V versus Li/Li^+), while V_2O_5 can access the lower bound (down to ~1.56 V versus Li/Li^+). Figure S15 reveals the redox mechanism of the LMO- V_2O_5 electrode pair. For LMO, the oxidation peaks are located at 4.2 and 4.4 V, while the corresponding reduction peaks in the reverse scan positively shift by 0.2 and 0.1 V, respectively, which is attributed to polarization as reported in organic electrolyte systems (51). For the V_2O_5 anode, the CV plot shows a multistep lithiation process. During the reduction scan, transitions are observed for V_2O_5 to $\alpha\text{-Li}_x\text{V}_2\text{O}_5$ ($0 < x < 0.01$) at 3.7 V, followed by $\epsilon\text{-Li}_x\text{V}_2\text{O}_5$ ($0.35 < x < 0.7$) at 3.4 V, $\delta\text{-Li}_x\text{V}_2\text{O}_5$ ($0.7 < x < 1$) at 3.2 V, and $\gamma\text{-Li}_x\text{V}_2\text{O}_5$ ($1 < x < 2$) at 2.3 V as lithiation proceeds. In the reverse scan, the corresponding oxidation peaks suggest a reversible de-lithiation process similar to previously reports in carbonate-based organic electrolyte systems (52). These results suggest that the extended ESW of WZH electrolyte maximizes the utilization of the available

Li storage site of V_2O_5 that is otherwise inaccessible in dilute solution or conventional hydrogels.

The performance of the WZH electrolyte is first evaluated in rigid full Li-ion cells comprising LMO as cathode, V_2O_5 as anode, and hydrogel electrolyte pre-equilibrated at RH of 50% as shown in fig. S16. Conductive silver ink (Dupont, PE 873), carbon ink (Dupont, PE 671) and active material slurries are printed via a stencil mask onto the polyethylene terephthalate (PET) film in a layer-by-layer fashion to form electrodes, while the cell stack is sealed between two glass substrates. Typical galvanostatic cycling with the potential limitation (GCPL) profiles of as fabricated full Li-ion cell is shown in fig. S17 with a specific capacity of $\approx 65 \text{ mAh g}^{-1}$ (based on both electrodes) with clear discharge plateaus at ~1.5 and ~0.5 V, which downshifts around 0.2 V as compared to previously reported works (27) due to the polarization of the homemade printed film collector instead of metal collector. Although the fabrication, assembly, and testing processes are performed in the ambient with the hydrogel pre-equilibrated at RH of 50%, the resulting battery reaches a high average CE of 97% at a slow rate of 0.2 C for over 200 charge-discharge cycles and a long operation time of over 1000 hours (fig. S18). This highlights the high reversibility of the redox reaction enabled by the extended ESW of the WZH electrolyte. After 200 cycles, the specific capacity is stabilized at 26 mAh g^{-1} , and the fading in capacity can be attributed to the mechanisms that are intrinsic to the V_2O_5 systems as reported in recent literature (53), which could be addressed by using other anode materials to potentially fully use the lower limit of the ESW such as Mo_6S_8 and TiS_2 (26, 54).

Stretchable aqueous Li-ion battery

The aqueous hydrogel electrolyte has good tolerance to moisture as water is part of the electrolyte system such that there is no need to use rigid packaging materials for hermetic sealing. A prototype stretchable Li-ion battery has been developed as shown in Fig. 4A, where the hydrogel is used as both the electrolyte and separator due to its excellent electrochemical stability, ion conductivity, and mechanical properties. The hydrogel with encircling stretchable elastomer VHB (very high bond; 3M 4905) is sandwiched between two stretchable electrode layers consisting of stencil-printed current collectors and anode/cathode on VHB (Fig. 4B). Scanning electron microscopy (SEM) clearly shows the cross-sectional view of the electrode and the hydrogel (Fig. 4C), highlighting robust interfaces between electrolyte and electrode, as well as between the active materials and current collector stack to allow efficient transfer of ions and electrons from and to the redox reactions. To improve the stretchability of the printed current collector, a wavy configuration is introduced by a pre-stretch-and-release method (33, 55). Specifically, silver and carbon stretchable conductive ink and active material slurries are printed on a stainless-steel substrate as stretchable electrodes. Meanwhile, the VHB tape is stretched to 150% of its original length, and the stencil-printed collector is transferred to the pre-strained VHB tape by using a heat-release tape as the transfer medium. The adhesion force of the heat-release tape allows it to transfer the printed electrodes off the stainless-steel substrate. Upon heating, the adhesion between the electrode and tape diminishes, and the printed electrodes are released to the pre-strained VHB substrate. A compressive stress is induced to the electrode after releasing the pre-strained VHB substrate, which leads to wrinkling electrodes. The as-fabricated electrode with a mass loading of V_2O_5 at 2.4 mg cm^{-2} shows a low sheet resistance of $1.0 \pm 0.1 \text{ ohm}/\square$, which has less than 5% change for a strain up to 50% and is highly reversible with respect to

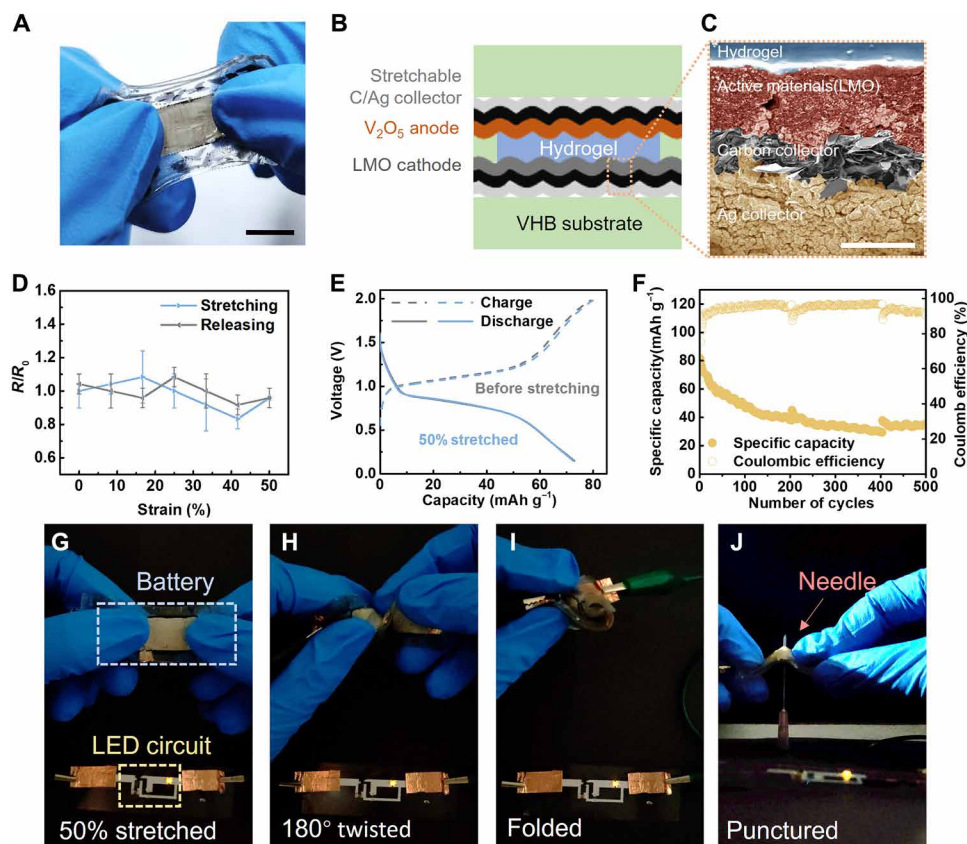


Fig. 4. Stretchable aqueous Li-ion battery. (A) An optical image of a stretchable aqueous Li-ion battery cell with WZH electrolyte and elastomer packaging. Scale bar, 1 cm. (B) Cross-sectional schematic view of the battery showing various layers. (C) SEM image showing the cross section of the electrode. Scale bar, 20 μm . (D) Normalized resistance of the V_2O_5 electrode as a function of stretching strain. (E) Galvanostatic cycling with potential limitation (GCPL) profile for a stretchable cell under 0% (gray color) and 50% (blue color) strain. (F) Evolution of specific capacity and coulomb efficiency of a cell over GCPL cycles at 1 C. Optical images showing the battery (two cells in series) powering to a circuit consisting of an LED and a dc-dc converter while being mechanically stressed: (G) 50% stretched, (H) 180° twisted, (I) folded, and (J) punctured by a needle.

strain variations (Fig. 4D). After 50 stretching cycles, the resistance increases by about 30% and remains stable for up to 100 stretching cycles (fig. S19). The full cell comprising stretchable LMO and V_2O_5 electrodes and WZH electrolyte demonstrates excellent capacity retention of $\sim 99\%$ when stretched with a 50% strain in the charge-discharge profile in Fig. 4E. The fabricated stretchable battery also shows good consistency across different samples in GCPL tests (tables S2 and S3) with an initial capacity of $69.6 \pm 9.6 \text{ mAh g}^{-1}$ at 1 C. The CE rises from $50.8 \pm 7.4\%$ for the 1st cycle to $90.9 \pm 4.0\%$ after 50th cycle. Meanwhile, the hydrogel-based electrolyte in combination with the elastomer package renders the cell with good ambient stability. GCPL tests are continuously performed for a full cell for a period of 1 month. Without the hermetic sealing, the prototype operates in the unstretched state at 1 C for 1 month in the ambient for 500 cycles with an average CE of 95% (Fig. 4F), which is substantially higher than those reported other similar systems (efficiency of ~ 70 to 80%) (27). After 250 cycles, the capacity stabilizes to reach around 36 mAh g^{-1} .

As a demonstration, we show that the printed prototype battery can light up a circuit composed of a direct current-to-direct current (dc-dc) converter, capacitors, and light-emitting diode (LED) under various mechanical stresses, including 50% stretching, 180° twisting, and folding (Fig. 4, G to I, and movie S1). Such deformable batteries could be desirable for practical usage in wearable electronics for good compliance with changes of the human body without limiting the

mobility to allow low-friction user-machine interactions. For wearable applications, chemical safety is also important as devices are deployed within high proximity to human skins. The nonflammable, fluorine-free hydrogel electrolyte demonstrated in this work can substantially reduce the chemical safety risks. Figure S20 shows that a prototype battery is completely cut through by a razor blade with exposed electrodes and hydrogel electrolyte. Because the hydrogel is in the quasi-solid state, the electrolyte layer maintains its original physical state without leaking. The non-reactivity of the aqueous electrolyte with respect to moisture avoids potentially hazardous conditions in contrast to organic electrolyte in conventional batteries, where leakage of electrolyte could cause violent hydrolytic reaction between organic Li salt and moisture. To illustrate the high mechanical robustness of the prototype battery, the battery is punctured through by a needle repeatedly while the prototype is powering the yellow LED module as demonstrated in Fig. 4J and movie S2. The puncturing is repeated for five times at different locations and the device can deliver power continuously for the LED module in the whole process.

Self-healable Li-ion battery and electronic system

In addition to promoting Li-ion dissociation for enhanced ESW, zwitterionic groups on the polymer backbone also synergize with carboxyl groups to form multiple sets of reversible cross-links, endowing WZH with good self-healing capability. In prior work (33), the self-healing

behavior of WZH has been studied under various conditions to explain possible mechanisms. Specifically, the self-healing process proceeds in two steps: (i) the instant reformation of reversible bonds and (ii) the subsequent migration of polymer chains across the wounded interface. These reversible bonds include ionic interactions between negatively charged sulfonic/deprotonated carboxyl groups and positively charged quaternary ammonium groups, as well as hydrogen bonds between acceptors (sulfonic and ester carbonyl groups) and donors (carboxyl groups). A schematic illustration of these interactions is shown in Fig. 5A. These reversible bonds can be repeatedly formed after mechanical damages to enable multiple self-healing cycles and ion-transporting channels are hence reestablished, which leads to a quick recovery of conductivity. Figure 5B shows the real-time resistivity change of the WZH after being cut through by a razor blade and subsequently healed 10 times at the same location. It can be seen that the hydrogel could recover to its original state with <10% change in resistance after each healing cycle. The combination of the self-healable hydrogel as the electrolyte and self-healable elastomer as the package renders good self-healing ability to the battery. Under severe damages such as the through cut in fig. S21, the battery shows good self-healing capability. SEM image on the healed region indicates good recovery for both the substrate layer and the electrolyte layer (Fig. 5C). After the through-cut process by a razor blade and the self-healing process at 70°C for 10 min, the battery regains about 90% of its original capacity (Fig. 5D) and restores good stretchability to exhibit similar performances as compared to that of a pristine device (fig. S22).

The battery has demonstrated good mechanical safety under damages, good stretchability/deformability, and self-healing ability such that it could potentially be used as the energy-embodied substrate to construct a self-healing soft electronic system. As a proof of concept, a stretchable and self-healing electronic system consisting of printed stretchable interconnects and off-the-shelf surface mounted devices (SMDs) including a dc-dc converter, capacitors, and an LED is integrated on top of the self-healing stretchable battery system consisting of cells in series connections (Fig. 5E). The stretchable interconnects are fabricated by transfer-printing stretchable conductive ink composed of liquid metal particles onto the self-healable elastomer substrate using a previously reported method (56). The system shows good conformality to non-flat surfaces such as human wrist and soft pneumatic actuator (fig. S23), which is highly desired as embodied power source for wearable electronics and soft robot applications. To demonstrate the system-level self-healing capability, a razor blade is used to cut through the whole system, including the stretchable interconnects and Li-ion cells. After cutting, the quasi-solid-state nature of the hydrogel prevents leakage even when the battery is cut in half, while the aqueous electrolyte ensures nonflammability of the system. After the system is healed at 70°C for 10 min and recharged, it remains functional to power the LED (Fig. 5F). Notably, the healed electronic system remains fully functional while enduring deformations such as flexing or twisting during operations as shown in Fig. 5G and movie S3.

DISCUSSION

This work presents a WZH electrolyte that can realize a high ESW of up to 3.11 V in ambient air without a rigid hermetic package. By exploiting the strong interactions between lithiophilic zwitterionic groups with lithium salt through the anti-polyelectrolyte effect, the

number of water molecules coordinated around the lithium ion is reduced. The free water molecules are further stabilized by functional groups on the zwitterionic polymer backbone through hydration and hydrogen bonding such that the reactivity of water molecules is minimized. The hygroscopic lithium salt is loaded in a controlled fashion with a small amount water content in balance with the ambient humidity. In such water-scarce condition, water molecules compete with zwitterionic groups for lithium ions, freeing them from the polymer backbone for enhanced ion mobility. The high tolerance aqueous system to the moisture as compared to that of organic electrolyte has allowed the fabrication of printed full cell batteries facilely in the ambient without a glovebox. Without the hermetic package, a myriad of stretchable elastomers can be used to enable high stretchability for the full Li-ion cell, while high mechanical and chemical safety is also achieved attributed to the aqueous hydrogel electrolyte. As a proof of concept, a stretchable and self-healing elastomer is chosen as the packaging material to construct soft Li-ion batteries with good capacity retentions under mechanical stresses, including punctured holes by a needle. Furthermore, the prototype cell can recover over 90% of its capacity from a through cut by a razor blade via the self-healing process. One key future direction is to increase the energy density for practical applications by these following steps. First, the mass loading can be further increased by incorporating the 3D microporous architecture as electrodes for high specific surface areas. Second, the selection of cathode and anode can be explored to maximize the utilization of electrolyte ESW. Third, the operation voltage of the battery can be increased by further extending the ambient ESW through optimization in molecular design that reduces hygroscopicity and water reactivity and facilitates stable SEI formation. As such, other battery chemistries with increased energy densities [e.g., $\text{LiNi}_{0.5}\text{Mn}_{1.5}\text{O}_4$ / $\text{Li}_4\text{Ti}_5\text{O}_{12}$ (23), Lithium metal (42, 56), and Li-S (57, 58)] could potentially be accommodated. Nevertheless, this strategy enables the development of mechanically safe and deformable Li-ion batteries and could potentially be suitable for other energy storage devices such as supercapacitors (59, 60), Zn-ion batteries (50), and metal air batteries (61). Furthermore, this work also offers the possibility for high-throughput manufacturing under the ambient condition by roll-to-roll printing.

MATERIALS AND METHODS

WZH electrolyte synthesis

All chemicals were purchased from Sigma-Aldrich and used without further purification unless otherwise noted. WZH was synthesized by mixing AA (1.50 g) with different amount of MEDSAH (0.75 g for WZH-1 and 1.5 g for WZH-2) and LiCl (the salt to total monomer ratio is fixed at 1:2) in deionized (DI) water (LiCl concentration fixed at 0.2 g/g H_2O). The initiator, ammonium persulfate (fixed to 0.2 mol % of total monomer amount), and cross-linker, MBAA (fixed to 0.03 mol % of total monomer amount), were then added to form the precursor solution. After complete dissolution, the solution was bubbled with N_2 for 10 min to deplete O_2 , and the solution was poured into a polystyrene petri dish and heated at 50°C for 24 hours. Preparation for the SEI forming interphase precursor was prepared following procedures from the literature (42). Specifically, the 0.5 M lithium bis(trifluoromethane)sulfonimide and 10 wt % polyethylene oxide (average M_v 100,000) were mixed in 1,1,2,2-tetrafluoroethyl-2',2',2'-trifluoroethyl ether (Thermo Fisher Scientific)/dimethyl carbonate (volume ratio = 95:5) and heated at 70°C for 20 min under stirring.

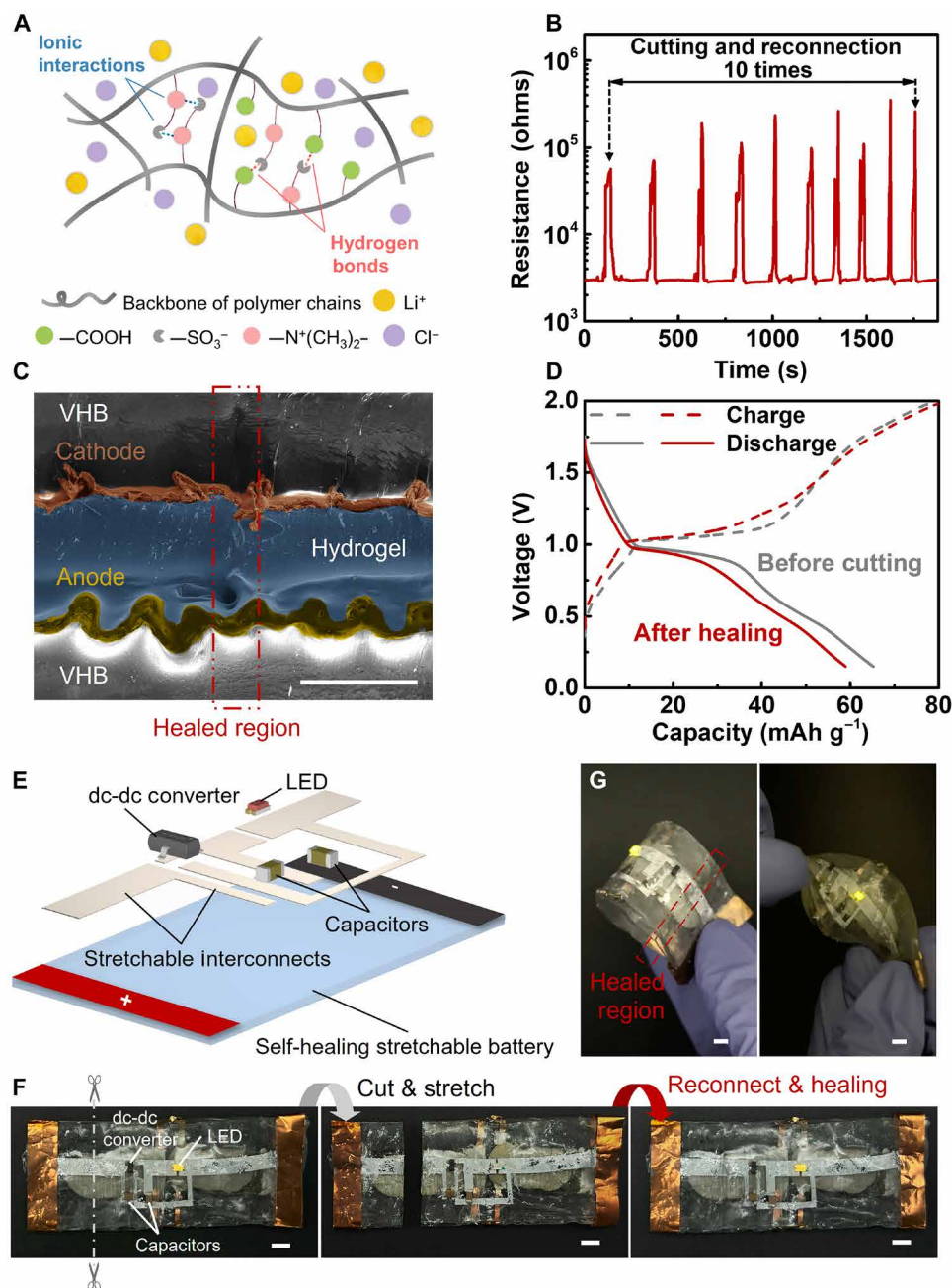


Fig. 5. Self-healable Li-ion battery and electronic system. (A) Schematic illustration of the reversible bonds in the WZH. (B) Resistivity changes with respect to time of the WZH sample for 10 through cuts and subsequently self-healing processes by a razor blade at room temperature. (C) SEM image showing the cross section of the prototype battery after being cut by a razor blade and a subsequent healing process at 70°C for 10 min. Healed region is highlighted by the dash-dotted line. Scale bar, 1 mm. (D) GCPL profiles for the pristine battery (gray color) and after a prototype is cut and put at 70°C for 10 min for the healing process (red color). Dashed lines represent voltage profiles during the charging process, and solid lines represent voltage profiles during the discharging process. (E) Schematic illustration of a self-healable electronic system comprising a substrate with embodied self-healing battery, printed stretchable interconnects, and SMD components including LED and capacitors. (F) The electronic system in its pristine state (left), after being cut through in halves by the razor blade (middle), and after the healing process at 70°C for 10 min and the recharging process (right). Scale bars, 5 mm. (G) Optical image showing the operation of electronic system under mechanical stresses such as folding (left) and twisting (right) after cutting and the subsequent self-healing process. Red dashed line highlights the healed region. Scale bars, 4 mm.

Electrode slurry preparation

For the preparation of the cathode slurry, a mixture of 0.8 g of LMO (MTI), 0.1 g of carbon black (SUPER C65, MSE Supplies), 2.5 g of a 2 wt % aqueous solution of carboxymethyl cellulose (CMC; MSE Supplies, average molecular weight \approx 600,000), and 0.33 g of polystyrene-butadiene rubber (PSBR; Targray Technology) solution were homogeneously mixed in DI water with zirconia beads in a planetary mixer (ARM 310, Thinky) at 2000 rpm for 30 min.

For the anode slurry, 0.7 g of vanadium pentoxide (V_2O_5 ; Sigma Aldrich), 0.2 g of carbon black, 2.5 g of 2 wt % CMC aqueous solution, 0.33 g of PSBR solution, and 1.49 ml of DI water were mixed with zirconia zirconium beads in a planetary mixer at 2000 rpm for 30 min.

Fabrication of rigid full Li-ion cells

A rigid full Li-ion cell comprises LMO as cathode, V_2O_5 as anode, and WZH as electrolyte. First, a stretchable silver ink (Dupont, PE 873) was printed via a stencil mask onto the PET film with a thickness of \sim 50 μ m and dried at 130°C for 10 min. Then, a layer of stretchable carbon ink (Dupont, PE 671; thickness \sim 50 μ m) was printed on top of a silver layer in the similar fashion. The printed carbon ink was then fully dried at 130°C for 15 min. The electrode slurry with active materials (LMO or V_2O_5) was printed on the dried carbon layer. The overall active material ratio between cathode and anode was kept at around 1.6:1, while the overall mass loading (cathode and anode) was around 6.2 mg cm^{-2} . The printed electrodes were then cut into strips with a width of \sim 5 mm. Before the rigid battery assembly, the glass slides were cut into squares with a width of 25 mm as the substrate and the superstrate for the full cell, and the hydrogels were cut into squares with a width of 10 mm. Then, the VHB tape (VHB 4910, 3 M) was cut into a square ring with an outer width of 25 mm and a square inside with a width of 10 mm to fit the hydrogel at the center. The rigid battery was then assembled by sequentially stacking electrodes, hydrogel with outer VHB ring, and glass superstrate on top of the bottom glass substrate as shown in fig. S16.

Stretchable battery fabrication

Wavy electrodes were prepared by first printing the stretchable silver ink (Dupont, PE 873) using a stencil mask on a stainless-steel substrate. This silver layer was then cured at 130°C for 5 min on a hot plate. Subsequently, a stretchable carbon ink (Dupont, PE 671) layer was printed using the same stencil printing method, and the carbon ink was cured at 130°C for 15 min on the hot plate. The electrode slurries were printed directly on top of the carbon layer and dried at 50°C for 30 min. The electrodes were transferred onto a heat release tape (Revalpha RA-95 L, Semiconductor Equipment Corp.) from the stainless-steel substrate and then transferred to a pre-stretched VHB substrate and heated at 105°C for 5 min to release the electrodes off the heat release tape. The SEI forming interphase precursor was applied to the anode using a doctor blade. Upon releasing the applied strain from the VHB substrate, a wavy structure is formed. The mass loading of the active layer was estimated by weighing the overall structure before and after printing the active layer. The overall active material ratio between cathode and anode was kept at around 1.6:1, while the overall mass loading (cathode and anode) was around 2.2 mg cm^{-2} . The battery was assembled by sandwiching the as-synthesized hydrogel (equilibrated in a chamber with a controlled humidity) between the prepared wavy electrodes.

Edges of the hydrogel were sealed by a perforated VHB, which also separated the cathode from the anode.

Characterizations

SEM images of the stretchable battery were obtained using a high-resolution field emission scanning electron microscope (FEI Quanta 3D FEG). HATR-FTIR spectra were performed on Spectrum One FTIR Spectrometer (PerkinElmer) with HATR sampling accessory, and Raman spectra were measured on LabRAM Aramis Raman Microscope (Horiba) with an excitation wavelength of 532 nm and diffraction grating of 1800 $g\ mm^{-1}$. DVS instrument (Surface Measurement Systems Ltd.) was used to characterize the sorption isotherms of hydrogels at different RHs (from 0 to 80%). The samples were preheated at 80°C, 0% RH for 5 hours, followed by thermal equilibrium at 25°C for 3 hours. The percent change of sample mass with respect to time was maintained at $0.005\%_{\text{sample}}\ \text{min}^{-1}$ at each RH for a precise measurement.

MD simulations

The simulation system comprises zwitterionic polymer chains, water molecules, and LiCl salts. The 3D gel network was constructed by physically cross-linking linear chains. First, each linear chain was built with a degree of polymerization of 12 (molecular weight of 5.08 kg/mol), wherein each monomer unit is made of one MEDSAH monomer and two AA monomers. Subsequently, 27 highly stretched chains were uniformly arranged within a cubic box in all three directions, e.g., 9 chains aligning along the z direction are uniformly distributed in the xy plane. A chemical bond was introduced between the head and tail atoms on the backbone of each chain across the periodic boundaries of the box. At a particular intersection in the x , y , and z directions, three chains meet. At this junction, a cross-linker is created by physically connecting identical types of carbon atoms on each chain (specifically, carbon atoms located in the middle of two adjacent AA monomers on the backbone). For each cross-linker, additional three bonds with an equilibrium bond length of 0.5 nm are added into the topology. The final 3D gel network is shown in fig. S5.

Mechanical and electrical characterizations

Hydrogel samples were prepared in a dog-bone shape (ISO 37, Type 3) using a tensile machine (Instron model 5544). A stretch rate of $2\ \text{min}^{-1}$ was used for extension-to-failure tensile tests. Cyclic tensile tests were performed in a similar fashion as reported by prior works (62, 63). Specifically, a strain rate of $0.2\ \text{s}^{-1}$ was used for loading and unloading the sample with a 2-min interval between cycles. The electrochemical impedances of the hydrogels were first measured using the electrochemical workstation (Gamry Reference 600) in a symmetric cell setup, where gold-coated PET films were used as inert electrodes. The ionic resistance of each sample was determined from the impedance with the phase shift near 0 degree. The measured resistance was converted to ionic conductivity

$$\sigma = \frac{l}{R(t \cdot w)} = \frac{l}{RA}$$

where l referred to the length of each hydrogel sample and A was the cross-sectional area (thickness times width) of each hydrogel. The area and thickness of each sample were measured and recorded before conducting each experiment. The resistance change of

stretchable electrodes under stretching was measured on a custom stretching stage by a digital multimeter (115, FLUKE). During measurements, two clamps were fixed on the two ends of the sample. The initial gauge length was defined as the separation gap between two clamps.

Electrochemical measurements

For the evaluation of the ESW of hydrogels, the linear sweep voltammetry on hydrogel was performed using a three-electrode setup with commercial screen-printed carbon electrodes (RRPE1001C, Pine Research Instrumentation) as the working and counter electrodes and Ag/AgCl as the reference electrode, and all hydrogel samples were pre-equilibrated in a chamber with RH of ~50%. A Gamry reference 600 electrochemical workstation was used for the linear sweep voltammogram measurements at a scan speed of 10 mV s⁻¹. For CV, the slurry was first obtained by mixing the active materials, conductive carbon (SUPER C65, MSE Supplies), and a binder (polyvinylidene difluoride, molecular weight of 534,000) in a weight ratio of 80:10:10, with *N*-methyl-2-pyrrolidone as the solvent in a planetary mixer (ARM 310, Thinky) at 2000 rpm for 30 min. The slurry was then coated onto glassy carbon electrode and dried at 60°C overnight. For the anode, an additional interphase precursor layer was coated onto the dried electrode. The coated glassy carbon electrode was used as the working electrode, Pt mesh as the counter electrode, and Ag/AgCl as the reference electrode. The CV measurements were done at a scan speed of 0.1 mV s⁻¹. The LMO/V₂O₅ full cell galvanostatic cycling was tested using a BCS series battery cycler (Bio-Logic SAS), while the impedance spectroscopy was measured on a Gamry Reference 600. To investigate the electrochemical performance of the cell under the mechanical strain, a custom-made stretching stage was used.

Fabrication of the self-healable electronic system

The circuitry was patterned on VHB tape using a transfer-printing method adopted from previous reports (33, 64, 65). First, eutectic gallium indium (eGaIn) liquid metal is prepared by melting a 3:1 mass ratio of gallium and indium (both from United Nuclear) mixture at a 180°C oven for 2 hours and then cool to room temperature. Next, stretchable conductive eGaIn ink was prepared by dispersing eGaIn and 1-Decanol (Sigma-Aldrich) at a 1:1 volume ratio and then homogenized using a probe sonicator (Qsonica Q700) at 200 W for 2 min. During sonication, the vial was placed in an ice-water bath, and the ultrasonication process operated in 5-s on/off cycles to prevent overheating. The obtained ink was printed onto a PET (Gizmo Dorks) substrate via a stencil mask (designed pattern was mirrored for transfer process) prepared using a mechanical cutting machine (Silhouette, CAMEO 3) and dried at 70°C for 10 min. The mask was then peeled off, and a VHB tape was pressed onto the PET substrate to allow close contact between the printed eGaIn interconnects and the VHB tape. The PET was then peeled off to transfer the liquid metal pattern. SMDs including a dc-dc converter (TPS7A10, Texas Instruments), capacitors (YAGEO), and an LED (*V*_{on} of ~1.8 V, SMT 1206, CHANZON) were then mounted on top of the VHB substrate using a silver epoxy (8331D, MG Chemicals) and further cured at 50°C for 30 min. Thereafter, the system was completed by assembling the circuitry layer on top of the battery module consisting of three cells in series and heated at 70°C for 15 min to allow sufficient interlayer bonding.

Supplementary Materials

The PDF file includes:

Supplementary Text
Figs. S1 to S23
Tables S1 to S3
Legends for movies S1 to S3
References

Other Supplementary Material for this manuscript includes the following:

Movies S1 to S3

REFERENCES AND NOTES

1. A. M. Zamarayeva, A. E. Ostfeld, M. Wang, J. K. Doney, I. Deckman, B. P. Lechêne, G. Davies, D. A. Steingart, A. C. Arias, Flexible and stretchable power sources for wearable electronics. *Sci. Adv.* **3**, e1602051 (2017).
2. R. Liu, Z. L. Wang, K. Fukuda, T. Someya, Flexible self-charging power sources. *Nat. Rev. Mater.* **7**, 870–886 (2022).
3. C. Lu, H. Jiang, X. Cheng, J. He, Y. Long, Y. Chang, X. Gong, K. Zhang, J. Li, Z. Zhu, J. Wu, J. Wang, Y. Zheng, X. Shi, L. Ye, M. Liao, X. Sun, B. Wang, P. Chen, Y. Wang, H. Peng, High-performance fibre battery with polymer gel electrolyte. *Nature* **629**, 86–91 (2024).
4. S. I. Rich, R. J. Wood, C. Majidi, Untethered soft robotics. *Nat. Electron.* **1**, 102–112 (2018).
5. F. Dai, M. Cai, Best practices in lithium battery cell preparation and evaluation. *Commun. Mater.* **3**, 64 (2022).
6. S. Xu, Y. Zhang, J. Cho, J. Lee, X. Huang, L. Jia, J. A. Fan, Y. Su, J. Su, H. Zhang, H. Cheng, B. Lu, C. Yu, C. Chuang, T.-I. Kim, T. Song, K. Shigeta, S. Kang, C. Dagdeviren, I. Petrov, P. V. Braun, Y. Huang, U. Paik, J. A. Rogers, Stretchable batteries with self-similar serpentine interconnects and integrated wireless recharging systems. *Nat. Commun.* **4**, 1543 (2013).
7. D. G. Mackanic, X. Yan, Q. Zhang, N. Matsuhashi, Z. Yu, Y. Jiang, T. Manika, J. Lopez, H. Yan, K. Liu, X. Chen, Y. Cui, Z. Bao, Decoupling of mechanical properties and ionic conductivity in supramolecular lithium ion conductors. *Nat. Commun.* **10**, 5384 (2019).
8. S. Y. Hong, S. M. Jee, Y. Ko, J. Cho, K. H. Lee, B. Yeom, H. Kim, J. G. Son, Intrinsically stretchable and printable lithium-ion battery for free-form configuration. *ACS Nano* **16**, 2271–2281 (2022).
9. D. G. Mackanic, M. Kao, Z. Bao, Enabling deformable and stretchable batteries. *Adv. Energy Mater.* **10**, 2001424 (2020).
10. C. Yang, Z. Suo, Hydrogel ionotronics. *Nat. Rev. Mater.* **3**, 125–142 (2018).
11. P. Le Floch, X. Yao, Q. Liu, Z. Wang, G. Nian, Y. Sun, L. Jia, Z. Suo, Wearable and washable conductors for active textiles. *ACS Appl. Mater. Interfaces* **9**, 25542–25552 (2017).
12. T. Ye, J. Wang, Y. Jiao, L. Li, E. He, L. Wang, Y. Li, Y. Yun, D. Li, J. Lu, H. Chen, Q. Li, F. Li, R. Gao, H. Peng, Y. Zhang, A tissue-like soft all-hydrogel battery. *Adv. Mater.* **34**, 2105120 (2022).
13. R. Kumar, J. Shin, L. Yin, J.-M. You, Y. S. Meng, J. Wang, All-printed, stretchable Zn-Ag₂O rechargeable battery via hyperelastic binder for self-powering wearable electronics. *Adv. Energy Mater.* **7**, 1602096 (2017).
14. C. Gu, M. Wang, K. Zhang, J. Li, Y.-L. Lu, Y. Cui, Y. Zhang, C.-S. Liu, A full-device autonomous self-healing stretchable soft battery from self-bonded eutectogels. *Adv. Mater.* **35**, 2208392 (2023).
15. S. Huang, L. Hou, T. Li, Y. Jiao, P. Wu, Antifreezing hydrogel electrolyte with ternary hydrogen bonding for high-performance zinc-ion batteries. *Adv. Mater.* **34**, 2110140 (2022).
16. T. Liu, X. Chen, E. Tervoort, T. Kraus, M. Niederberger, Design and fabrication of transparent and stretchable zinc ion batteries. *ACS Appl. Energy Mater.* **4**, 6166–6179 (2021).
17. M. Gu, W. J. Song, J. Hong, S. Y. Kim, T. J. Shin, N. A. Kotov, S. Park, B. S. Kim, Stretchable batteries with gradient multilayer conductors. *Sci. Adv.* **5**, eaaw1879 (2019).
18. S. Huang, F. Wan, S. Bi, J. Zhu, Z. Niu, J. Chen, A self-healing integrated all-in-one zinc-ion battery. *Angew. Chem. Int. Ed. Engl.* **131**, 4357–4361 (2019).
19. W.-J. Song, J. Park, D. H. Kim, S. Bae, M.-J. Kwak, M. Shin, S. Kim, S. Choi, J.-H. Jang, T. M. Shin, S. Y. Kim, K. Seo, S. Park, Jabuticaba-inspired hybrid carbon filler/polymer electrode for use in highly stretchable aqueous Li-ion batteries. *Adv. Energy Mater.* **8**, 1702478 (2018).
20. J. Pu, Q. Cao, Y. Gao, Q. Wang, Z. Geng, L. Cao, F. Bu, N. Yang, C. Guan, Liquid metal-based stable and stretchable Zn-ion battery for electronic textiles. *Adv. Mater.* **36**, 2305812 (2024).
21. X. Xiao, X. Xiao, Y. Zhou, X. Zhao, G. Chen, Z. Liu, Z. Wang, C. Lu, M. Hu, A. Nashalian, S. Shen, K. Xie, W. Yang, Y. Gong, W. Ding, P. Servati, C. Han, S. X. Dou, W. Li, J. Chen, An ultrathin rechargeable solid-state zinc ion fiber battery for electronic textiles. *Sci. Adv.* **7**, eabl3742 (2021).
22. F. Wang, O. Borodin, M. S. Ding, M. Gobet, J. Vatamanu, X. Fan, T. Gao, N. Eidson, Y. Liang, W. Sun, S. Greenbaum, K. Xu, C. Wang, Hybrid aqueous/non-aqueous electrolyte for safe and high-energy Li-ion batteries. *Joule* **2**, 927–937 (2018).

23. Y. Yamada, K. Usui, K. Sodeyama, S. Ko, Y. Tateyama, A. Yamada, Hydrate-melt electrolytes for high-energy-density aqueous batteries. *Nat. Energy* **1**, 16129 (2016).
24. M. R. Lukatskaya, J. I. Feldblyum, D. G. Mackanic, D. L. Lissel, D. L. Michels, Y. Cui, Z. Bao, Concentrated mixed cation acetate “water-in-salt” solutions as green and low-cost high voltage electrolytes for aqueous batteries. *Energy Environ. Sci.* **11**, 2876–2883 (2018).
25. L. Suo, O. Borodin, W. Sun, X. Fan, C. Yang, F. Wang, T. Gao, Z. Ma, M. Schroeder, A. von Cresce, S. M. Russell, M. Armand, A. Angell, K. Xu, C. Wang, Advanced high-voltage aqueous lithium-ion battery enabled by “water-in-bisalt” electrolyte. *Angew. Chem. Int. Ed. Engl.* **55**, 7136–7141 (2016).
26. L. Suo, O. Borodin, T. Gao, M. Olguin, J. Ho, X. Fan, C. Luo, C. Wang, K. Xu, “Water-in-salt” electrolyte enables high-voltage aqueous lithium-ion chemistries. *Science* **350**, 938–943 (2015).
27. X. Chen, H. Huang, L. Pan, T. Liu, M. Niederberger, Fully integrated design of a stretchable solid-state lithium-ion full battery. *Adv. Mater.* **31**, 1904648 (2019).
28. J. Zhang, C. Cui, P.-F. Wang, Q. Li, L. Chen, F. Han, T. Jin, S. Liu, H. Choudhary, S. R. Raghavan, N. Eidson, A. Cresce, L. Ma, J. Uddin, D. Addison, C. Yang, C. Wang, “Water-in-salt” polymer electrolyte for Li-ion batteries. *Energy Environ. Sci.* **13**, 2878–2887 (2020).
29. X. Hou, T. P. Pollard, X. He, L. Du, X. Ju, W. Zhao, M. Li, J. Wang, E. Paillard, H. Lin, J. Sun, K. Xu, O. Borodin, M. Winter, J. Li, “Water-in-eutectogel” electrolytes for quasi-solid-state aqueous lithium-ion batteries. *Adv. Energy Mater.* **12**, 2200401 (2022).
30. X. He, B. Yan, X. Zhang, Z. Liu, D. Bresser, J. Wang, R. Wang, X. Cao, Y. Su, H. Jia, C. P. Grey, H. Frielinghaus, D. G. Truhlar, M. Winter, J. Li, E. Paillard, Fluorine-free water-in-ionomer electrolytes for sustainable lithium-ion batteries. *Nat. Commun.* **9**, 5320 (2018).
31. Y. Wang, Q. Li, H. Hong, S. Yang, R. Zhang, X. Wang, X. Jin, B. Xiong, S. Bai, C. Zhi, Lean-water hydrogel electrolyte for zinc ion batteries. *Nat. Commun.* **14**, 3890 (2023).
32. S. Xiao, Y. Zhang, M. Shen, F. Chen, P. Fan, M. Zhong, B. Ren, J. Yang, J. Zheng, Structural dependence of salt-responsive polyelectrolyte brushes with an anti-polyelectrolyte effect. *Langmuir* **34**, 97–105 (2018).
33. P. He, Y. Long, C. Fang, C. H. Ahn, A. Lee, C.-M. Chen, J. H. Park, M. Wang, S. K. Ghosh, W. Qiu, R. Guo, R. Xu, Z. Shao, Y. Peng, L. Zhang, B. Mi, J. Zhong, L. Lin, Moisture self-regulating ionic skins with ultra-long ambient stability for self-healing energy and sensing systems. *Nano Energy* **128**, 109858 (2024).
34. W. Zhang, B. Wu, S. Sun, P. Wu, Skin-like mechanoresponsive self-healing ionic elastomer from supramolecular zwitterionic network. *Nat. Commun.* **12**, 4082 (2021).
35. N. Wang, X. Yang, X. Zhang, Ultrarobust subzero healable materials enabled by polyphenol nano-assemblies. *Nat. Commun.* **14**, 814 (2023).
36. B. Auer, R. Kumar, J. R. Schmidt, J. L. Skinner, Hydrogen bonding and Raman, IR, and 2D-IR spectroscopy of dilute HOD in liquid D₂O. *Proc. Natl. Acad. Sci. U.S.A.* **104**, 14215–14220 (2007).
37. B. M. Auer, J. L. Skinner, IR and Raman spectra of liquid water: Theory and interpretation. *J. Chem. Phys.* **128**, 224511 (2008).
38. J. Xie, Z. Liang, Y.-C. Lu, Molecular crowding electrolytes for high-voltage aqueous batteries. *Nat. Mater.* **19**, 1006–1011 (2020).
39. M. E. Tuckerman, D. Marx, M. Parrinello, The nature and transport mechanism of hydrated hydroxide ions in aqueous solution. *Nature* **417**, 925–929 (2002).
40. J. Dong, Y. Ozaki, K. Nakashima, Infrared, Raman, and near-infrared spectroscopic evidence for the coexistence of various hydrogen-bond forms in poly(acrylic acid). *Macromolecules* **30**, 1111–1117 (1997).
41. J. Xu, X. Ji, J. Zhang, C. Yang, P. Wang, S. Liu, K. Ludwig, F. Chen, P. Kofinas, C. Wang, Aqueous electrolyte design for super-stable 2.5 V LiMn₂O₄ || Li₄Ti₅O₁₂ pouch cells. *Nat. Energy* **7**, 186–193 (2022).
42. C. Yang, J. Chen, T. Qing, X. Fan, W. Sun, A. von Cresce, M. S. Ding, O. Borodin, J. Vatamanu, M. A. Schroeder, N. Eidson, C. Wang, K. Xu, 4.0 V aqueous Li-ion batteries. *Joule* **1**, 122–132 (2017).
43. C. Liu, J. Qi, B. He, H. Zhang, J. Ju, X. Yao, Ionic conductive gels based on deep eutectic solvents. *Int. J. Smart Nano Mater.* **12**, 337–350 (2021).
44. S. Huang, F. Wan, S. Bi, J. Zhu, Z. Niu, J. Chen, A self-healing integrated all-in-one zinc-ion battery. *Angew. Chem. Int. Ed. Engl.* **58**, 4313–4317 (2019).
45. Y. Hu, R. Shi, Y. Ren, W. Peng, C. Feng, Y. Zhao, S. Zheng, W. Li, Z. Sun, J. Guo, S. Guo, X. Wang, F. Yan, A “Two-in-One” strategy for flexible aqueous batteries operated at –80°C. *Adv. Funct. Mater.* **32**, 2203081 (2022).
46. X. Zhou, S. Huang, L. Gao, Z. Zhang, Q. Wang, Z. Hu, X. Lin, Y. Li, Z. Lin, Y. Zhang, Y. Li, X. Li, J. Chen, Molecular bridging induced anti-salting-out effect enabling high ionic conductive ZnSO₄-based hydrogel for quasi-solid-state zinc ion batteries. *Angew. Chem. Int. Ed. Engl.* **63**, e202410434 (2024).
47. Y. Liu, F. Li, J. Hao, H. Li, S. Zhang, J. Mao, T. Zhou, R. Wang, L. Zhang, C. Zhang, A polyanionic hydrogel electrolyte with ion selective permeability for building ultra-stable Zn//Li batteries with 100°C wide temperature range. *Adv. Funct. Mater.* **34**, 2400517 (2024).
48. M. Sun, G. Ji, M. Li, J. Zheng, A robust hydrogel electrolyte with ultrahigh ion transference number derived from zincophilic “chain-gear” network structure for dendrite-free aqueous zinc ion battery. *Adv. Funct. Mater.* **34**, 2402004 (2024).
49. T. Liu, X. Du, H. Wu, Y. Ren, J. Wang, H. Wang, Z. Chen, J. Zhao, G. Cui, A bio-inspired methylation approach to salt-concentrated hydrogel electrolytes for long-life rechargeable batteries. *Angew. Chem. Int. Ed. Engl.* **135**, e202311589 (2023).
50. Y. Yan, S. Duan, B. Liu, S. Wu, Y. Alsaied, B. Yao, S. Nandi, Y. Du, T. W. Wang, Y. Li, X. He, Tough hydrogel electrolytes for anti-freezing zinc-ion batteries. *Adv. Mater.* **35**, e2211673 (2023).
51. J. Guo, Y. Chen, C. Xu, Y. Li, S. Deng, H. Xu, Q. Su, Enhanced electrochemical performance of LiMn₂O₄ by SiO₂ modifying via electrostatic attraction forces method. *Ionics (Kiel)* **25**, 2977–2985 (2019).
52. J. M. Cocciantelli, J. P. Doumerc, M. Pouchard, M. Broussely, J. Labat, Crystal chemistry of electrochemically inserted LiV₂O₅. *J. Power Sources* **34**, 103–111 (1991).
53. X. Hou, L. Zhang, N. Gogoi, K. Edström, E. J. Berg, Interfacial chemistry in aqueous lithium-ion batteries: A case study of V₂O₅ in dilute aqueous electrolytes. *Small* **20**, 2308577 (2024).
54. W. Sun, L. Suo, F. Wang, N. Eidson, C. Yang, F. Han, Z. Ma, T. Gao, M. Zhu, C. Wang, “Water-in-salt” electrolyte enabled LiMn₂O₄/TiS₂ lithium-ion batteries. *Electrochem. Commun.* **82**, 71–74 (2017).
55. S. Yan, G. Zhang, H. Jiang, F. Li, L. Zhang, Y. Xia, Z. Wang, Y. Wu, H. Li, Highly stretchable room-temperature self-healing conductors based on wrinkled graphene films for flexible electronics. *ACS Appl. Mater. Interfaces* **11**, 10736–10744 (2019).
56. Z. Gao, N. Song, Y. Zhang, X. Li, Cotton-textile-enabled, flexible lithium-ion batteries with enhanced capacity and extended lifespan. *Nano Lett.* **15**, 8194–8203 (2015).
57. N. Song, Z. Gao, Y. Zhang, X. Li, B₄C nanoskeleton enabled, flexible lithium-sulfur batteries. *Nano Energy* **58**, 30–39 (2019).
58. Z. Gao, Y. Zhang, N. Song, X. Li, Towards flexible lithium-sulfur battery from natural cotton textile. *Electrochim. Acta* **246**, 507–516 (2017).
59. L. Bao, X. Li, Towards textile energy storage from cotton T-shirts. *Adv. Mater.* **24**, 3246–3252 (2012).
60. Z. Gao, C. Bumgardner, N. Song, Y. Zhang, J. Li, X. Li, Cotton-textile-enabled flexible self-sustaining power packs via roll-to-roll fabrication. *Nat. Commun.* **7**, 11586 (2016).
61. Y. Xu, Y. Ang Zhao, J. Ing Ren, Y. Zhang, H. Peng, An all-solid-state fiber-shaped aluminum-air battery with flexibility, stretchability, and high electrochemical performance. *Angew. Chem. Int. Ed. Engl.* **55**, 7979–7982 (2016).
62. Y. Wang, C. Zhu, R. Pfattner, H. Yan, L. Jin, S. Chen, F. Molina-Lopez, F. Lissel, J. Liu, N. I. Babiah, Z. Chen, J. W. Chung, C. Linder, M. F. Toney, B. Murmann, Z. Bao, A highly stretchable, transparent, and conductive polymer. *Sci. Adv.* **3**, 1602076 (2017).
63. S. Zhang, Y. Zhou, A. Libanori, Y. Deng, M. Liu, M. Zhou, H. Qu, X. Zhao, P. Zheng, Y.-L. Zhu, J. Chen, S. C. Tan, Biomimetic spinning of soft functional fibres via spontaneous phase separation. *Nat. Electron.* **6**, 338–348 (2023).
64. R. Xu, P. He, G. Lan, K. Behrouzi, Y. Peng, D. Wang, T. Jiang, A. Lee, Y. Long, L. Lin, Facile fabrication of multilayer stretchable electronics via a two-mode mechanical cutting process. *ACS Nano* **16**, 1533–1546 (2022).
65. Z. Wang, K.-C. Lei, H. Tang, Y. Luo, H. Zhao, P. He, W. Ding, L. Lin, Stretchable liquid metal e-skin for soft robot proprioceptive vibration sensing. *IEEE Sens. J.* **24**, 18327–18335 (2024).
66. S. Jo, T. Kim, V. G. Iyer, W. Im, CHARMM-GUI: A web-based graphical user interface for CHARMM. *J. Comput. Chem.* **29**, 1859–1865 (2008).
67. J. Huang, A. D. MacKerell Jr., CHARMM36 all-atom additive protein force field: Validation based on comparison to NMR data. *J. Comput. Chem.* **34**, 2135–2145 (2013).
68. M. J. Abraham, T. Murtola, R. Schulz, S. Páll, J. C. Smith, B. Hess, E. Lindahl, GROMACS: High-performance molecular simulations through multi-level parallelism from laptops to supercomputers. *SoftwareX* **1–2**, 19–25 (2015).
69. S. Miyamoto, P. A. Kollman, SETTLE: An analytical version of the SHAKE and RATTLE algorithm for rigid water models. *J. Comput. Chem.* **13**, 952–962 (1992).
70. G. Bussi, D. Donadio, M. Parrinello, Canonical sampling through velocity rescaling. *J. Chem. Phys.* **126**, 014101 (2007).
71. H. J. C. Berendsen, J. P. M. van Postma, W. F. Van Gunsteren, A. DiNola, J. R. Haak, Molecular dynamics with coupling to an external bath. *J. Chem. Phys.* **81**, 3684–3690 (1984).
72. T. Darden, D. York, L. Pedersen, Particle mesh Ewald: An N³/log(M) method for Ewald sums in large systems. *J. Chem. Phys.* **98**, 10089–10092 (1993).
73. K. Liu, M. G. Brown, C. Carter, R. J. Saykally, J. K. Gregory, D. C. Clary, Characterization of a cage form of the water hexamer. *Nature* **381**, 501–503 (1996).

Acknowledgments: We thank Y. Qin at University of Oxford for the help with schematic rendering. We also want to express our appreciation for G. Lau and A. Kusoglu at Lawrence Berkeley National Laboratory for the kind help with dynamic vapor adsorption test.

Funding: This work is supported, in part, by Bakar Fellows Program (L.S. and P.H.). Work was performed, in part, at the Biomolecular Nanotechnology Centre (BNC) laboratory and Marvell Nanofabrication Laboratory at the University of California, Berkeley, and at the Molecular

Foundry, Lawrence Berkeley National Laboratory. Work at the Molecular Foundry was supported by the Office of Science, Office of Basic Energy Sciences, of the US Department of Energy under contract no. DE-AC02-05CH11231. A few of authors get support from Berkeley Sensor and Actuator Center. Work at the Hong Kong University of Science and Technology (Guangzhou) was supported by the startup grant (G0101000199) (C.F.). **Author contributions:** Conceptualization: P.H., Y.P., and Y.L. Methodology: P.H., J.H.P., Y.J., R.G., Y.H., M.W., Y.P., and A.T. Investigation: P.H., J.H.P., Y.J., R.G., Y.H., A.L., C.H.A., M.W., Y.P., Y.L., C.-M.C., Z.W., and Z.T. Visualization: P.H. and C.F. Supervision: B.M., A.C.A., C.F., A.T., and L.L. Writing—original draft: P.H., J.H.P., Y.J., R.G., Y.H., and C.F. Writing—review and editing: C.F., A.T., and L.L. **Competing interests:** P.H., Y.P.,

Y.L., and L.L. are inventors on US patent application (US 2024/0332613 A1) held by University of California that covers reconfigurable soft lithium-ion battery. The authors declare that they have no other competing interests. **Data and materials availability:** All data needed to evaluate the conclusions in the paper are present in the paper and/or the Supplementary Materials.

Submitted 6 November 2024

Accepted 5 March 2025

Published 9 April 2025

10.1126/sciadv.adu3711